N-35
2239

NASA Contractor Report 189701

Radiometric Infrared Focal [illegible] Plane Array Imaging System for Thermographic Applications

B. J. Es[illegible]
N. Mc[illegible]
F. [illegible]
[illegible]
W. F. K[illegible]

David Sarnoff Research Center
and
*New [illegible] Technology

Contract [illegible]

NA[illegible]

Contents

Figures

Figures (concluded)

PREFACE

This final report was prepared by the David Sarnoff Research Center (Sarnoff), Princeton, NJ, under Contract No. NAS1-18226. It describes work performed for the period November 11, 1991 to June 30, 1992, in the Optoelectronics Research Laboratory, Gary W. Hughes, Director. The work was performed as a collaborative effort between Sarnoff and the New Jersey Institute of Technology (NJIT), Newark, NJ. The Program Manager was John R. Tower, Head, Solid State Imaging at Sarnoff. Additional programmatic support was provided by Robert Brown, of SRI International, Menlo Park, CA. The Project Scientist at Sarnoff was Benjamin J. Esposito.

Walter F. Kosonocky, Distinguished Professor of Electrical Engineering and holder of the NJIT Chair for Optoelectronics and Solid State Circuits, was the Project Scientist for the NJIT effort. Dr. Kosonocky was previously employed at Sarnoff from 1955 until 1987 and is currently a senior consultant to Sarnoff in the Solid State Imaging Group. Nathaniel J. McCaffrey, a graduate student working under the direction of Dr. Kosonocky, was responsible for characterization of the PtSi FPA radiometric performance.

1.0 INTRODUCTION

This document describes research performed under *The Radiometric Infrared Focal Plane Array Imaging System for Thermographic Applications* contract. This research investigated the feasibility of using platinum silicide (PtSi) Schottky-barrier infrared focal plane arrays (IR FPAs) for NASA Langley's specific radiometric thermal imaging requirements. The initial goal of this design was to develop a high spatial resolution radiometer with a temperature resolution of 1% of the temperature reading over the range of 0 to 250°C. The proposed camera design developed during this study and described in this report provides: 1) high spatial resolution (full-TV resolution); 2) high thermal dynamic range (0 to 250°C); 3) the ability to image rapid, large thermal transients utilizing electronic exposure control (commandable dynamic range of 2,500,000:1 with exposure control latency of 33 ms); 4) high uniformity (0.5% nonuniformity after correction); and 5) high thermal resolution (0.1°·C at 25°C background and 0.5°C at 250°C background).

Sarnoff's 640 x 480 IR FPA was chosen as the image sensor for the work performed during this contract. The contract was divided into three specific tasks. Task 1 evaluated the spectral and broadband uniformity of the existing 640 x 480 PtSi camera system by experimental procedures. Task 2 evaluated the radiometric characteristics of the 640 x 480 camera system by comparing the measured results to the radiometric requirements and computer simulations. Results obtained under Tasks 1 and 2 are provided in Section 2. These results were analyzed during Task 3 to form a basis for the proposed design and specification for a high performance radiometer. Section 3 describes the proposed design and specification of a 640 x 480 PtSi Schottky-barrier IR FPA camera system for use as a high resolution radiometer.

2.0 RADIOMETRIC EVALUATION

A theoretical and experimental study was made of the radiometric characteristics of the Sarnoff 640 x 480 IR-MOS imager for developing an IR camera system for thermographic applications. The expected performance parameters of the imaging radiometer such as the temperature resolution and the required integration time were evaluated by computer analysis and verified by experiments. However, the imager characteristics such as the linearity, uniformity, and stability were determined by direct testing of the imager.

2.1 TEST MEASUREMENT SYSTEM

The experimental tests were performed at the David Sarnoff Research Center, Princeton, New Jersey between March 15 and June 15, 1992. The test camera was fabricated early into the project's development. The camera head consisted of a 640 X 480 infrared FPA mounted in an LN_2 cooled dewar assembly and two (2) printed circuit (PC) boards mounted on the camera chassis. The PC boards contain the electronics that supply clocking pulses, correlated double sampling of the output video, signal conditioning, and power to the FPA.

Figure 1 shows the test camera integrated into the primary evaluation system (additional equipment was utilized for some of the testing). The test apparatus consisted of a square radiator, a filter wheel, a current picoammeter, a data acquisition unit, two video digitizers, an Apple MAC IIfx computer, and *FrameGrabber* software. These units were consolidated under the computer's control to work as the characterization system. The black body source, an Electro Optical Industries (BH2450E) large aperture radiator (with a range of 25 to 170°C), was controlled and monitored using an IEEE-488 interface. Two video digitizers were employed to convert the odd and even video fields into computer data. The test setup was controlled by a computer utilizing software developed at Sarnoff. *FrameGrabber* is a flexible, high speed, data acquisition software system developed specifically for the characterization of solid state imaging arrays. The video signal is captured and analyzed using a Macintosh graphical interface. *FrameGrabber* can print the captured image, generate defect lists and uniformity histograms, and calculate multiplicative correction coefficients that can be applied to any acquired frame.

The filter wheel shown in Fig. 1 was not used in this experiment. To obtain more accurate measurements, optical bandpass filters were placed inside the dewar assembly (to limit radiation leakage and the thermal radiation of the filters) as is shown in Fig. 2. The dewar window passes all wavelengths above 3.5 μm. The baffle limits the field of view and also suppresses internal reflections. The baffle assembly also acts as a mount for neutral density and band pass filters. Neutral density filters were employed to attenuate high temperature signals so that the signal reaching the detector does not exceed the saturation output signal of the detectors (roughly 1×10^6 electrons/pixel).

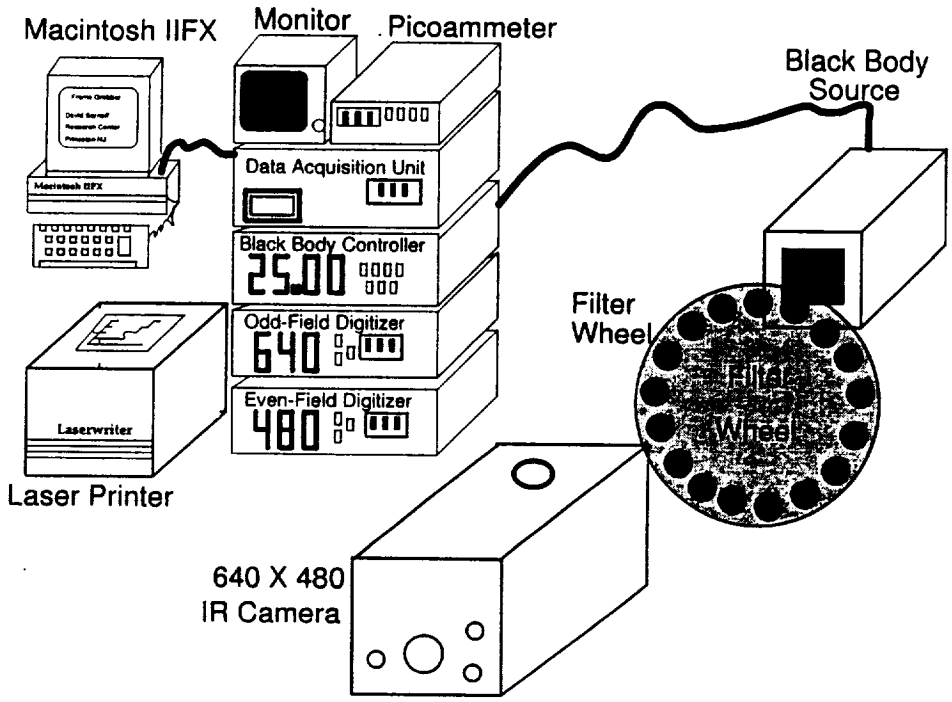

Figure 1. Test camera integrated into the primary evaluation system (additional equipment was utilized for some of the testing).

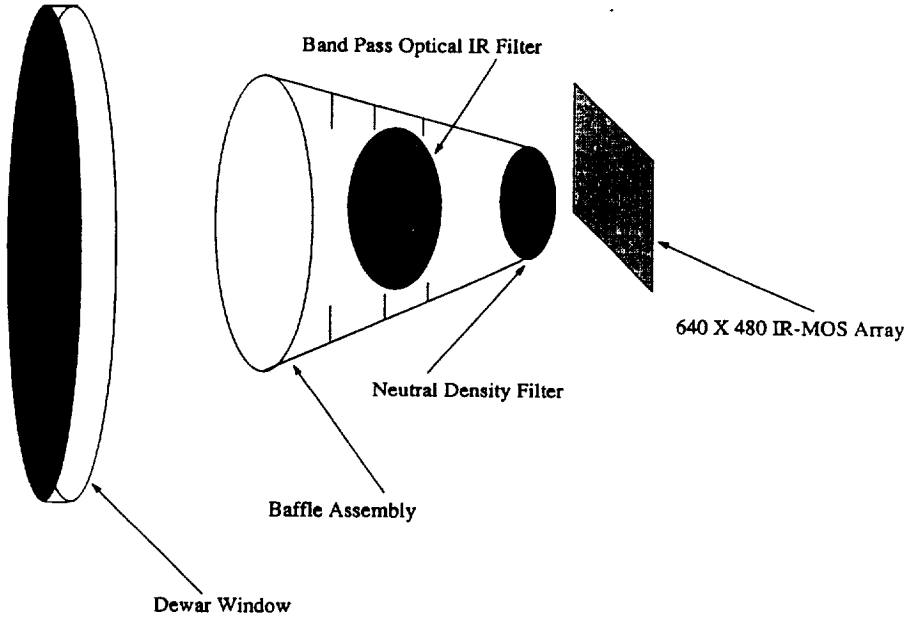

Figure 2. Optical Assembly. To obtain more accurate measurements, optical bandpass filters were placed inside the dewar assembly (to limit radiation leakage and the thermal radiation of the filters).

2.2 LINEARITY

The output electrical signal response to changes in the input optical signal were evaluated. The detector array was uniformly illuminated with various temperatures of blackbody radiation and the photoresponse was measured. The relationship between optical power and radiated temperature was explored. Response linearity measurements were made at integration times of 0.25, 0.75, and 33 ms.

2.2.1 Radiance Calculations

Blackbodies emit thermal electromagnetic radiation in accordance with the Planck law:

$$M_{e,\lambda}(\lambda,T) = \frac{2\pi hc^2}{\lambda^5\left[e^{hc/\lambda kT}-1\right]} = \frac{3.74 \times 10^4 \ \mathrm{Wcm}^2}{\lambda^5\left[e^{14{,}388/\lambda T}-1\right]} \qquad (1)$$

where

$M_{e,\lambda}(\lambda,T)$ = spectral radiant exitance in watts per square centimeter of area and micrometer of radiation wavelength ($W \cdot cm^{-2} \cdot \mu m^{-1}$),

λ = blackbody radiation wavelength in micrometers (μm),

T = blackbody temperature in Kelvin (°K),

k = Boltzmann's constant,

c = speed of light (3×10^{10} cm·sec^{-1}),

h = Planck's constant (6.626×10^{-34} W·sec^2).

The camera system limits the useful incident radiation to the bandwidth between 3.5 and 5.5 μm. The 3.5-μm cuton is due to the long pass characteristics of the cold filter. The 5.5 μm cutoff is due to the response of the PtSi detectors. Therefore, the useful incident radiated power density can be found by evaluating:

$$M_e(T) = \int_{\lambda_2}^{\lambda_1} \frac{3.74 \times 10^4}{\lambda^5\left[e^{14{,}388/\lambda T}-1\right]}\, d\lambda \qquad (2)$$

The solution of the above equation was obtained by numerical analysis using a trapezoidal integration with $\Delta\lambda = 0.01$ μm and limits of $\lambda_1 = 3.5$ μm and $\lambda_2 = 5.5$ μm. From this relation, we can predict the camera response to changes in the exitance of a blackbody source.

2.2.2 Test Results

The IR test camera was integrated into the test setup and data from the FPA in uncorrected format was digitized and stored for analysis by the *Frame Grabber* software. Frames were acquired by uniformly illuminating the imager with temperatures ranging from 18 to 150°C at the standard 33 ms integration time (full frame). The average drain current at these temperatures was also recorded. From the stored frames, the response of individual pixels to changes in temperature can be evaluated.

Figure 3 shows the response in electrons/pixel to changes in scene temperatures ranging from 15 to 55°C for ten pixels whose positions were chosen to sample the entire area of the array. A second order response is clearly shown and the slightly irregular responses illustrate the nonuniformities of the array. The pixels are described in the legend using the format [lin(x,y)], where the x and y coordinates represent the absolute location of the pixel on the array with lin(1,1) in the top left-hand corner of the screen.

Figure 4a is a plot of the measured drain current in nA to changes in the blackbody temperature. The plot shows that at <80°C, the signal is unsaturated and the current has a second order response with temperature with $^{dI}/_{dT}$=0.548T -3.045 [$^{nA}/_{°C}$]. At >80°C, the optical signal saturates the detector and any increase in temperature yields negligible increase in the drain current. Figure 4b shows the relationship between measured drain current and applied optical signal. The plot shows a linear rise followed by an abrupt saturation at 1812 nA. The optical power to induce saturation at full frame integration is ~5 $^{mW}/_{cm^2}$ measured as the blackbody output exitance. Closer inspection of the linear region shows deviations at both ends. In the region near saturation, the current changes less than expected. In the low power region, the detected current tends to remain constant. However tests with cold neutral density filters indicate that the deviation of linearity at low light levels is mainly due to the background and dark currents. Shown in the inset of Fig. 4b is the fractional error of the signal from linearity as a function of exitance. The error in linear response for optical signals ranging from 1.7 to 3.7 $^{mW}/_{cm^2}$ is < ±0.3%.

To properly calibrate and characterize the camera for further studies, the output voltage as a function of temperature was studied. Figure 5 shows the relationships between the detector signal in electrons/pixel and the RS-170 video output voltage in millivolts to variations in the blackbody temperature. The video voltage measurement was taken after impedance matching the oscilloscope to the 75 Ω coaxial line. Figure 6 provides a conversion from the average RS-170 output voltage measurement to the average charge in electrons/pixel collected by the PtSi detectors. From the results of the measurements shown in Fig. 6, a transconduction gain was calculated to be 806 electrons/pixel/mV.

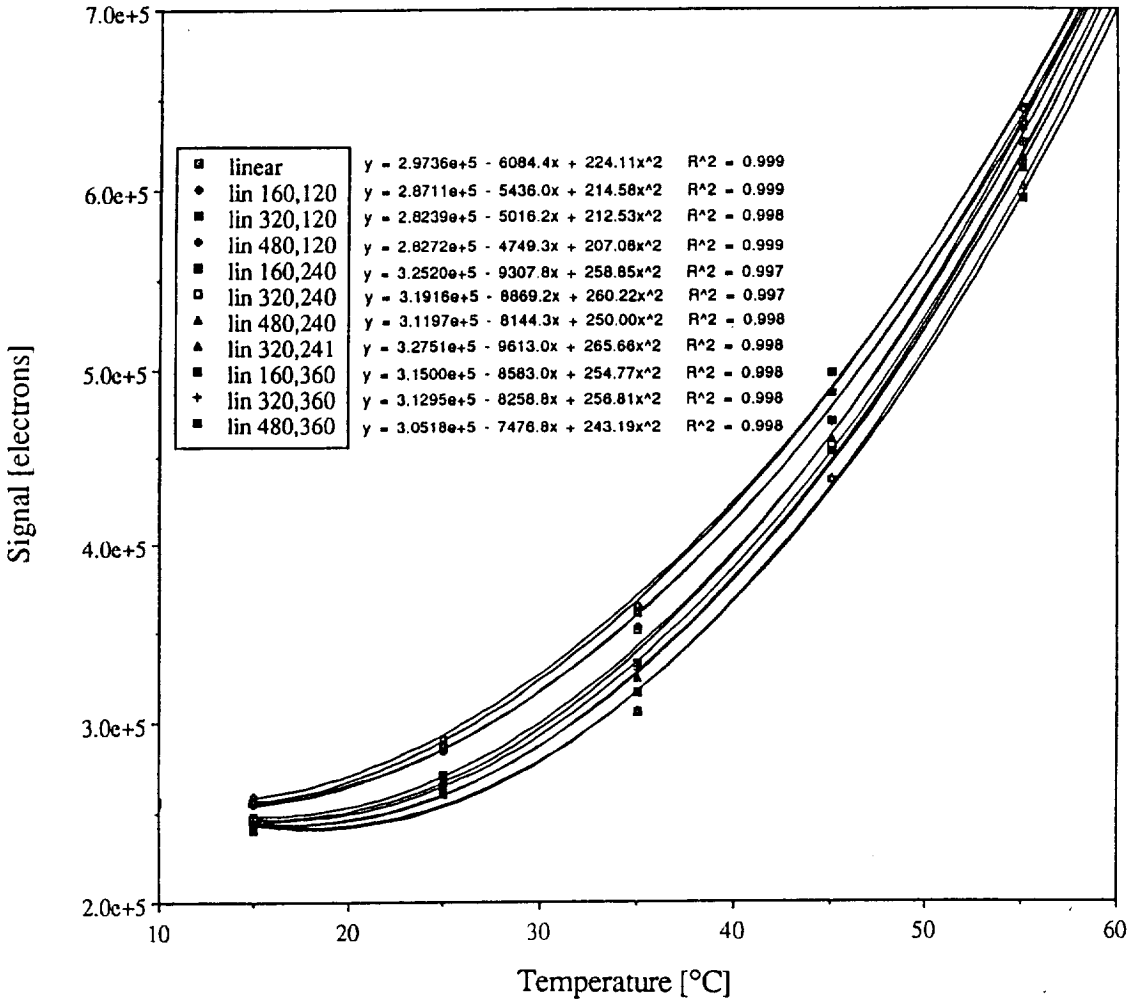

Figure 3. Detected pixel signal vs temperature. The response in electrons/pixel to changes in scene temperatures ranging from 15 to 55 °C for ten pixels whose positions were chosen to sample the entire area of the array.

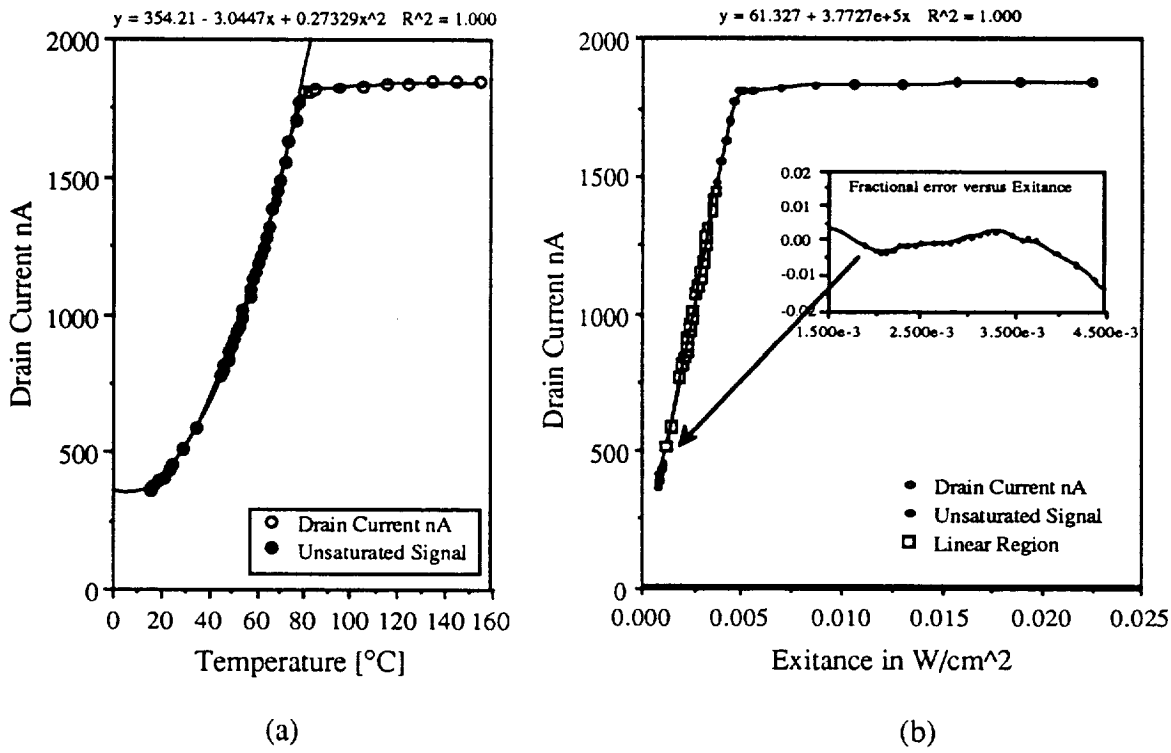

Figure 4. a) Plot of the measured drain current in nA to changes in the blackbody temperature and b) the relationship between measured drain current and applied optical signal. The inset in Fig. 4b shows the fractional error of the signal from linearity as a function of exitance.

To accurately measure temperatures exceeding the saturation signal of the imager, the optical integration time may be reduced. By reading and dumping the charge from detectors and subsequently reading and storing the detector signal a short time later, sub-frame rate charge integration can be realized. Two integration times of 12 and 4 horizontal line times were studied. The standard video horizontal line time is 63.5 μsec, which yields integration times of 762 μsec and 254 μsec respectively. Figure 7 shows the relationship between measured camera output voltage in millivolts to variations in blackbody temperature for the two reduced integration times studied. Also shown on the graph is the level at which the uniformly illuminated array saturates. This level is dependent on the reverse bias applied to the detectors and this bias is noted. The responses of the two curves differ in both slope and intercept. The lower integration time can be used to measure higher temperatures.

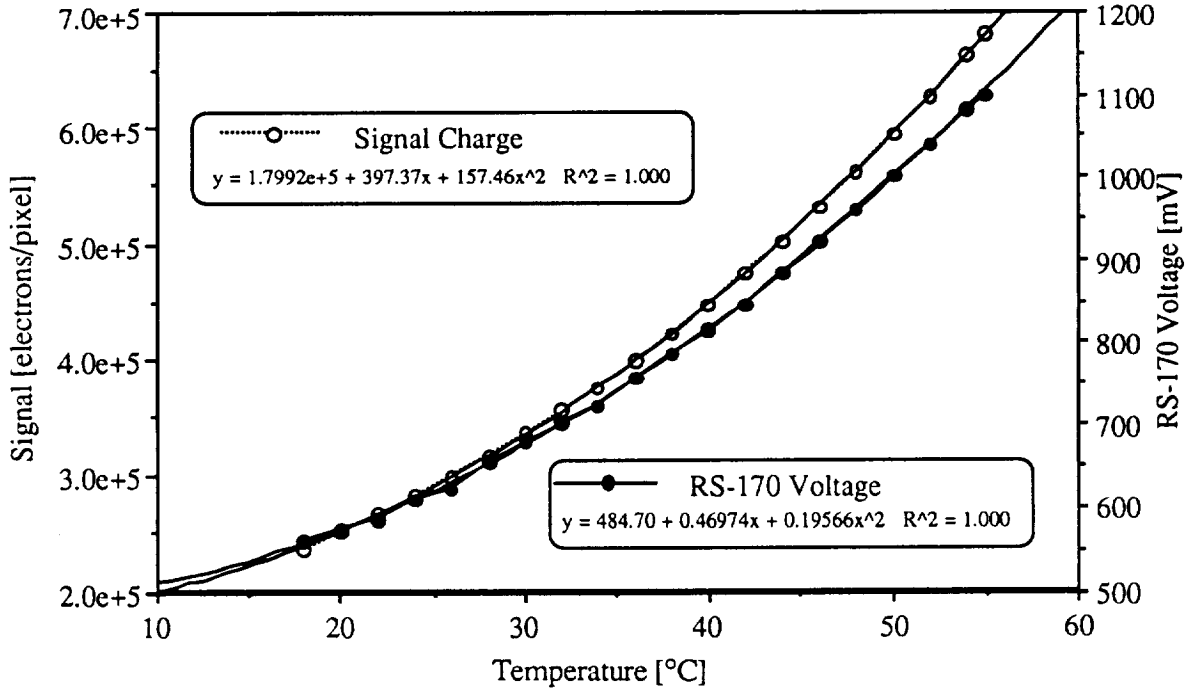

Figure 5. Camera output characteristics vs temperature for the 640 x 480 IR-MOS FPA.

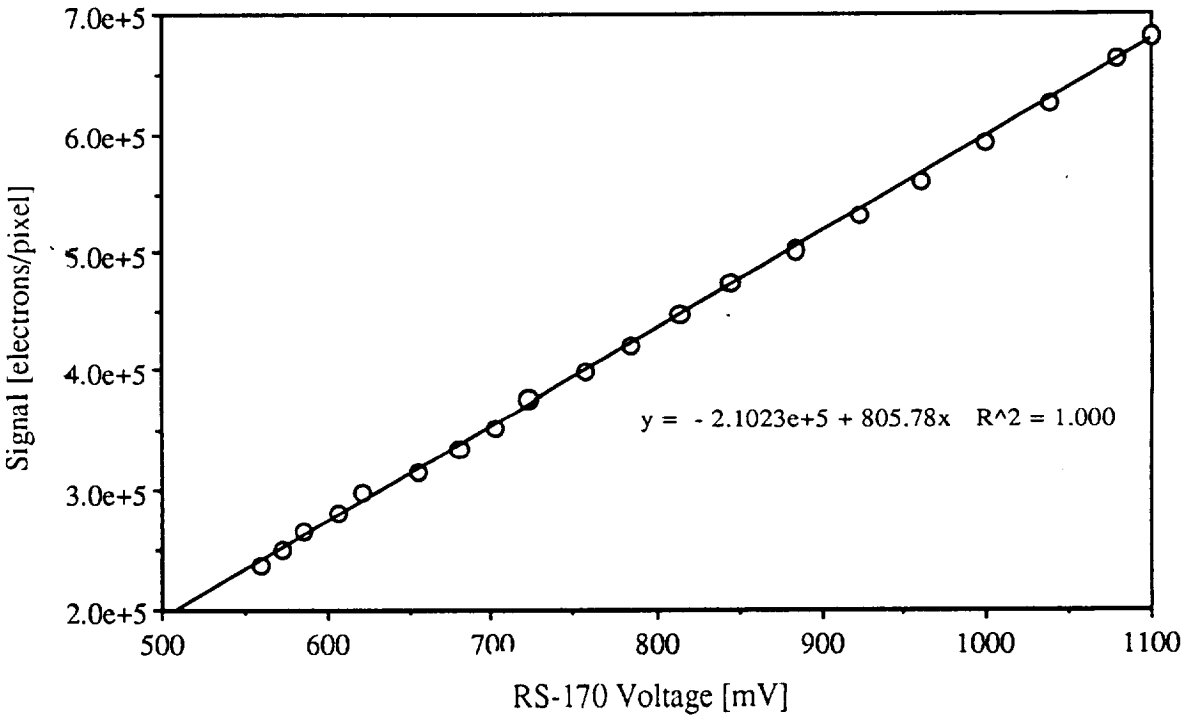

Figure 6. Transconduction gain of the 640 X 480 IR camera.

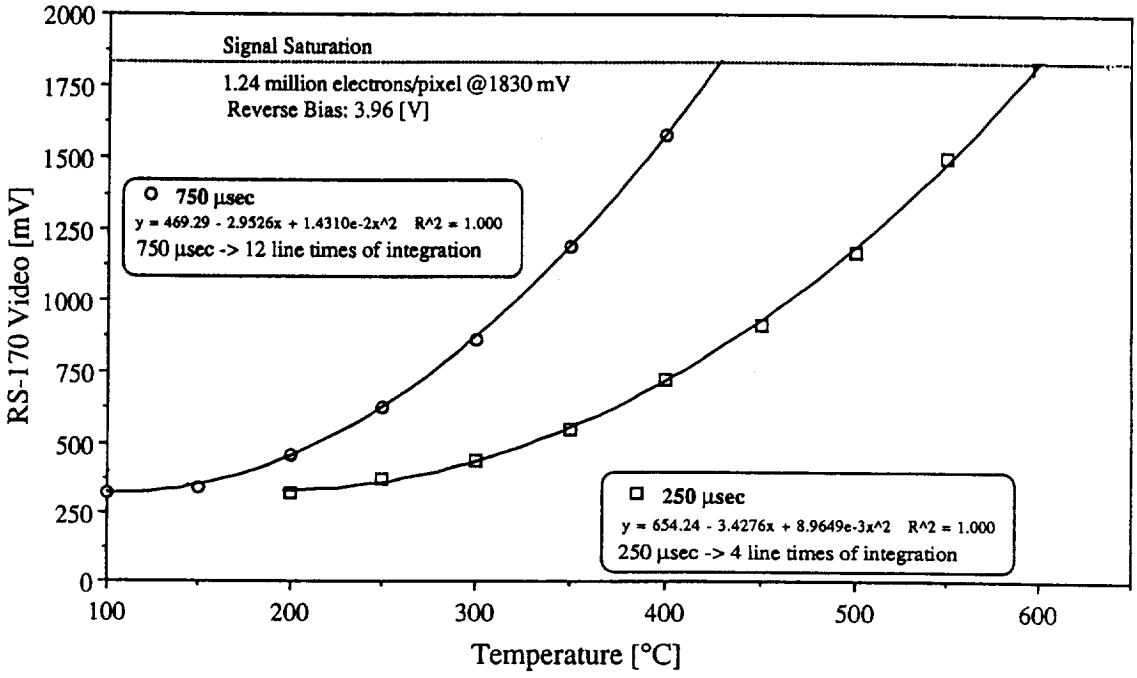

Figure 7. Output voltage vs temperature for 640 x 480 IR-MOS FPA at two short integration times.

Performing the same radiometric analysis as described above, the output voltage as a function of optical power was examined and is shown in Fig. 8a. Figure 8b shows that the camera system responds linearly with optical signal up to 1.2 $^{W}/_{cm^2}$ when a 250 µsec integration time is used.

2.3 THERMAL RESPONSE

2.3.1 Modelled Performance

As the temperature of an object increases, the emitted infrared optical power increases (following the Planck's Radiation Law). Photon gasses conform to Bose-Einstein statistics and this distribution determines the spectral signature of the signal. The peak of the spectral distribution varies with temperature following Wein's Displacement Law:

$$\lambda_m \cdot T^{-1} = 2897.8 \quad [\mu m \cdot (°K)^{-1}] \tag{3}$$

where

λ_m = wavelength at which the emission has its highest value,

T = temperature in °K.

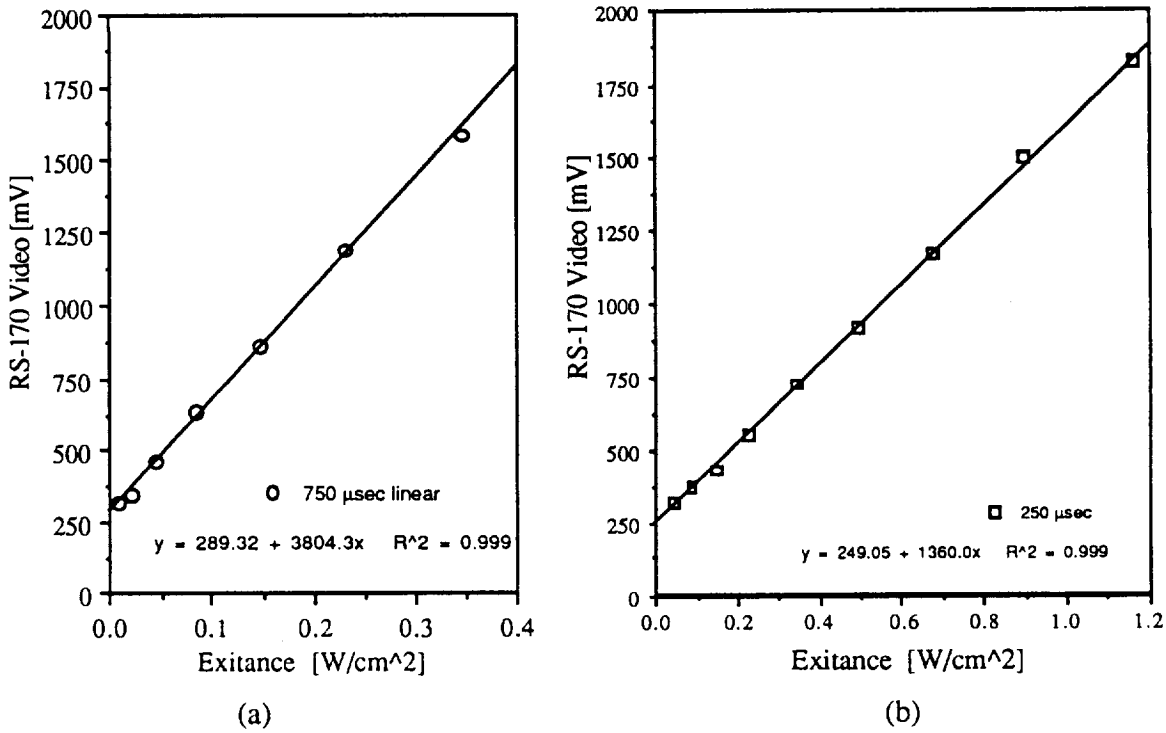

Figure 8. a) Output signal vs exitance for 750 µsec and b) 250 µsec.

As the peak of the optical power varies between 3.5 and 5.5 µm, variations in the spectral response from pixel to pixel would cause variations in the pixel to pixel thermal response.

The responsivity, R of a Schottky-barrier detector can be approximated by a Fowler equation as:

$$\mathfrak{R} = C_1\left[1-\left(\frac{\Psi_{ms}\bullet\lambda}{1.237}\right)\right]^2 \ A/W \qquad (4)$$

where:

R is the responsivity in (A/W),

λ is the wavelength of the incident infrared radiation in(µm),

C_1 is the quantum efficiency coefficient in (eV^{-1}), and

Ψ_{ms} is the metal-semiconductor barrier height in (eV).

Therefore, two quantities (C_1 & Ψ_{ms}) characterize the thermal response for each detector. By maintaining a constant temperature and filtering small bandwidths of the thermal radiation (for modelling monochromaticity), the responsivity of ten representative pixels were measured.

2.3.2 Test Results

Bandpass filters with sidebands of the order (±0.1 μm) were placed inside the dewar and a constant 150°C target temperature was maintained. Signals were acquired using *FrameGrabber* software and 16 frames were averaged to make a composite image with reduced temporal noise effects. This image was analyzed to yield measurements of the electrical output signal for ten representative pixels chosen to represent the entire area of the FPA. The spectral responsivity has been defined as the output diode current (based on conversion from voltage to equipment current) divided by the input optical power per unit wavelength. Figure 9 shows the spectral responsivity in A/W as a function of wavelength. Also shown is the spectral response of the average pixel. The data in Fig. 9 shows that the ten detectors sampled have practically identical responsivities for the wavelengths of interest (3.5 to 5.5 μm). The maximum deviation from the average was found to be ±1% at 3.7 microns. It is important to note that the spectral response characteristics of the ten detectors were very similar, thus indicating no measureable spectral nonuniformity. Therefore, pixel to pixel nonuniformities should not vary significantly with incident power spectral density.

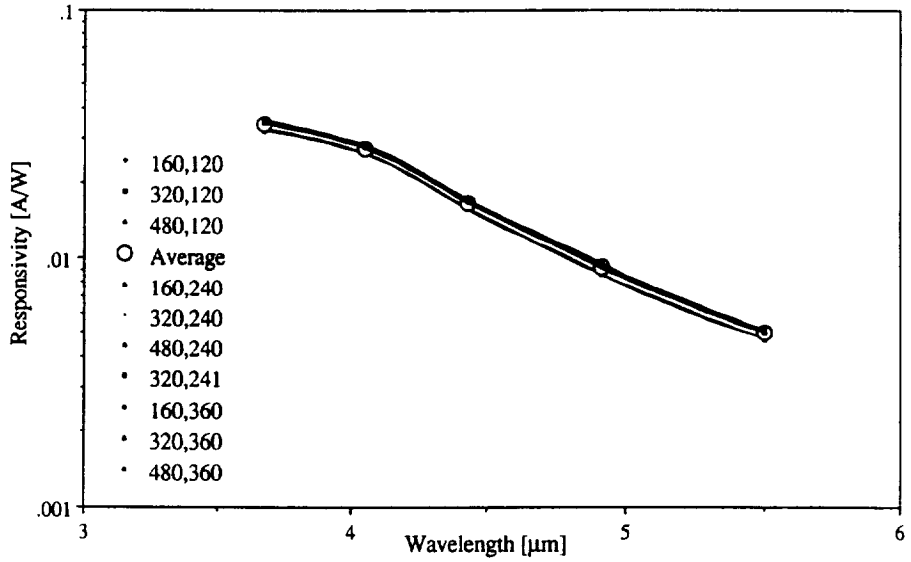

Figure 9. Spectral responsivity of the 640 x 480 IR imager for 10 representative pixels.

2.4 UNIFORMITY CORRECTION

When the camera is uniformly illuminated, the signal from each pixel in the array should be equal. Furthermore, any change in temperature ΔT should induce equal changes in the pixel signal ΔS. Due to inherent anomalies in the process of fabricating the imaging chip, nonuniformities in both the offset and slope of the pixel response are present. These nonuniformities need to be corrected for the chip to perform as a radiometer. Correcting for both the slope and offset of individual pixels in an array is called two point correction. Figure 10 shows graphically the procedure for obtaining two point correction. Part 1 shows the response of any arbitrary

uncorrected pixel (i) and the average response of the FPA for two reference temperatures T_1 and T_2. The offset has been subtracted in Part 2 at the temperature T_1 from all pixel responses. At this point, the only difference in pixel responses is due to their varying slopes. Gain coefficients are now computed which are used to force the differential response of each pixel to be the same as that of the average pixel. This is shown in Part 3. Illustrated in Part 4, to preserve the radiometric information, the same signal due to T_1 minus the dark current is added to the offset and gain corrected signal of Part 3.* The reinserted offset signal can be either average array signal or a local average signal near the center of the imager.

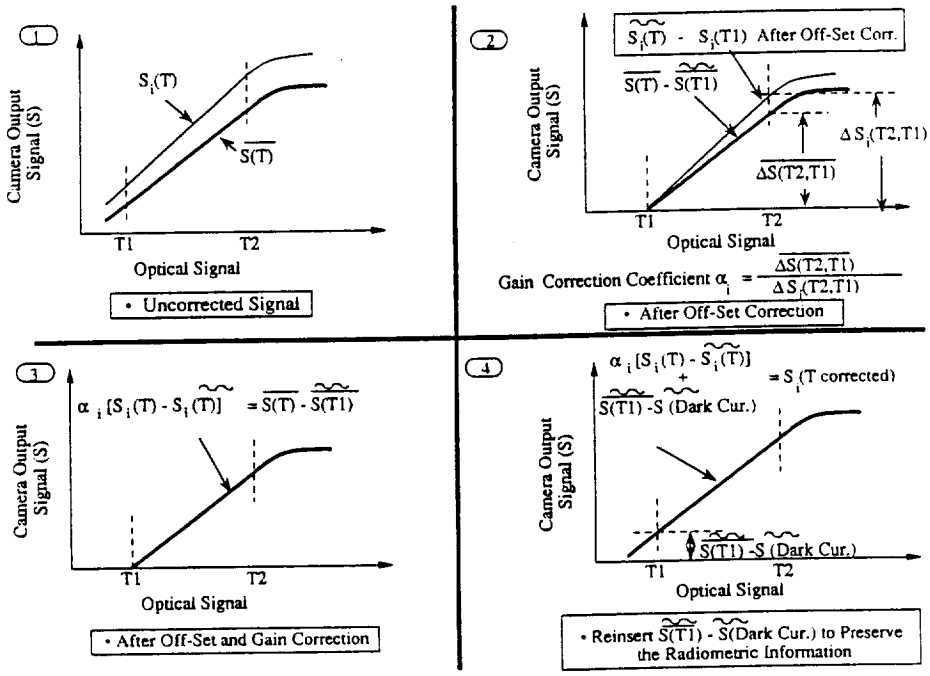

Figure 10. Procedure for obtaining two point correction.

2.4.1 Description for Test Procedure

Data was acquired by the *FrameGrabber* program at two temperatures (T_1 and $T_2=T_1 + 5°C$). A 20 frame average of the blackbody radiator scene was used to calculate the uniformity of the array. The mean was calculated as the average pixel amplitude of the scene. The response is the measured change in the amplitude of the pixel at the two different temperature scenes. The mean response is the average calculated response of the array. Percent deviations were calculated and the % rms nonuniformity was calculated from these deviations. Data was taken at temperatures ranging from 25 to 65°C at full frame integration and from 100 to 170°C at 750 μsec signal integration time. The

* The concept of one and/or two point uniformity correction preserving radiometric accuracy was proposed by W. F. Kosonocky of NJIT prior to this project.

camera used for this experiment was equipped with two point correction circuitry. The camera was offset corrected while staring at the blackbody radiator to remove irregularities in the emissivity of the square radiator if any were present. Multiplicative coefficients were generated to correct for nonuniformities encountered while staring at 25°C radiation and were stored in memory. These coefficients were applied to the signals acquired at the various temperatures of this experiment.

2.4.2 Test Results

Figure 11 illustrates the distributions of the array uniformities for the corrected camera. The histogram plot shows the percentage of pixels along the y-axis vs the percent deviation from the mean along the x-axis. The calculated mean is placed at the center of the x-axis and the number of pixels falling into equally sized bins around the mean are plotted in both directions away from the center. Bins to the left of the mean represent pixels whose displays are darker than average. Figure 11a shows the camera system behaving with high uniformity at the temperature where the coefficients were originally generated. This behavior is expected. As the signal level is increased in Figs. 11b ,c ,and d, the detectors respond similarly and the deviation of the pixel response increases only slightly. At >70°C however, as pixels begin to saturate, the nonuniformities increase dramatically. Also shown in Fig. 11d are two distinct peaks in the plot. This is thought to be due to the uneven responses of the two fields used in the interlaced mode. This deviation is small however.

Figure 12 shows the deviation from uniformity as a function of blackbody temperature for two integration times. Figure 12a illustrates the constant nonuniformity under 0.2% for temperatures between 30 to 65°C. In Fig. 12b, the nonuniformities as a function of temperature for a 750 μsec integration time are shown. The jump in nonuniformity has been attributed to the automatic switching of the camera into a lower gain mode when the integration time is changed for the camera used in this study. The test setup is calibrated to digitize signals with a greater range and the larger nonuniformity may be attributed to this fact. The shape of Fig.12b is similar to that of Fig. 12a showing an independence of the array nonuniformity to both temperature and signal level. Figure 13 shows the array nonuniformity expressed as an equivalent temperature difference as a function of incident temperature. The data was converted from percent rms variations of the output voltage into rms deviations in the measured temperature. Figure 13a shows that the deviant pixels vary from the mean response by a fraction of a degree to the point of pixel saturation. In Fig. 13b, the integration time has been reduced and as stated above, an automatic switch in the camera gain occurred. The large effective temperature deviation can be attributed to two factors. The rms nonuniformity was higher than at the low integration due to the gain switch and the range of the instrumentation as previously mentioned. Also, the signal level for this integration time for the temperature range of 100 to 140°C is very low. Under normal operation, to ideally measure temperatures in this range, a longer integration time of 0.005 seconds should be utilized.

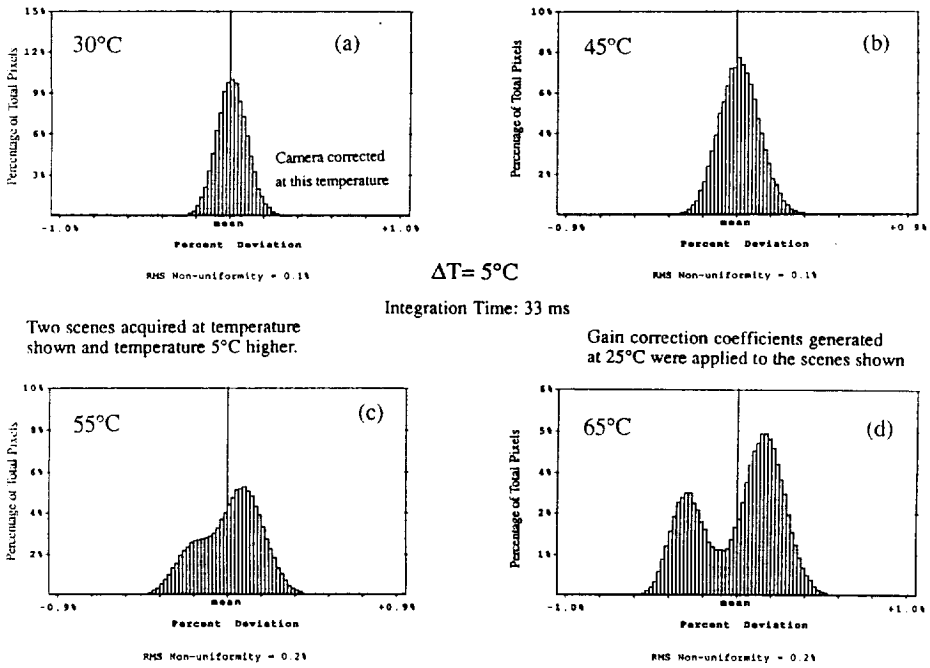

Figure 11. Uniformity of corrected 640 x 480 IR-MOS FPA with temperature.

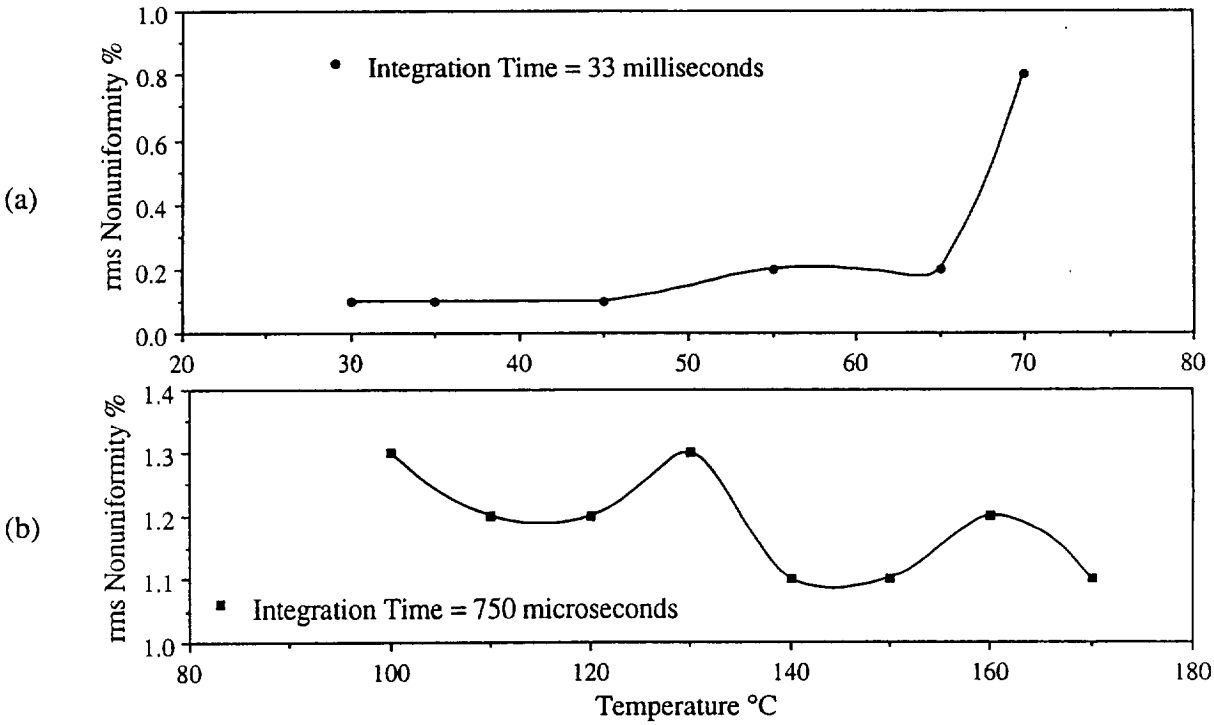

Figure 12. a) The constant nonuniformity under 0.2% between 30 to 65 °C. b) The nonuniformities as a function of temperature for a 750 μsec integration time.

(a)

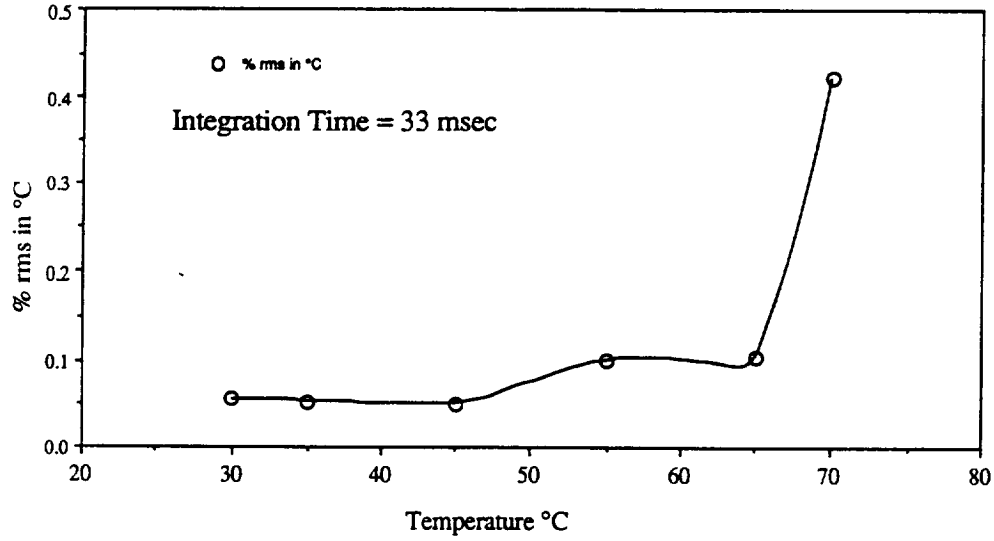

(b)

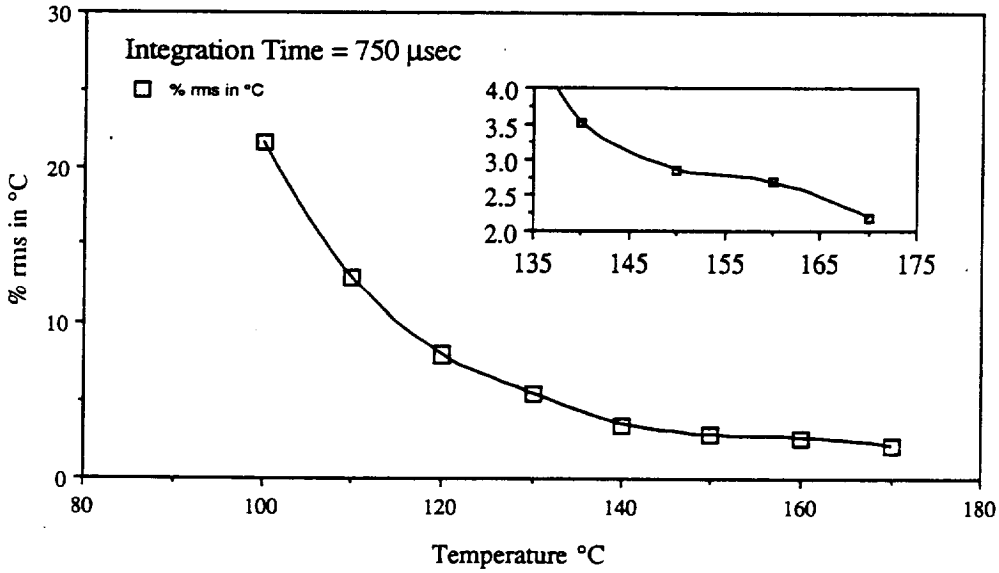

Figure 13. Array nonuniformity expressed as an equivalent temperature difference as a function of incident temperature.

2.5 NOISE EQUIVALENT DIFFERENTIAL TEMPERATURE (NEΔT)

The Noise Equivalent Differential Temperature (NEΔT) is a measure representing the total temporal pixel noise at a given background temperature converted into an equivalent temperature difference at the background scene. This is a widely used figure of merit for characterization of an infrared measuring system.

2.5.1 Radiometry

The NEΔT for an FPA is normally measured as:

$$NE\Delta T = {}^{N_{noise}}/_{\Delta N_B/\Delta T} \ (°K) \tag{5}$$

where:

N_{noise} = measured temporal noise at a pixel in $(rms \cdot {}^{electrons}/_{pixel})$,

$\Delta N_B/\Delta T$ = measured FPA responsivity in (electrons/pixel/°K) for a background signal N_B in electrons/pixel.

To correctly model the performance of the imager, the detected signal as well as the noise equivalent temperature must be calculated as a function of exposure. The signal detected by the imager viewing the blackbody radiator can be represented as:

$$S(T,t_i) = A_d \cdot \frac{\Pi}{4\left(f/_{\#}\right)^2} \cdot \frac{t_i}{1.602 \text{ X } 10^{-19}} \int_0^{\infty} \Re(\lambda)\, L_{\lambda,b}(\lambda,T)\, d\lambda \tag{6}$$

where:

$S(T,t_i)$ = signal at the output of the IR camera in (electrons/pixel),

$R(\lambda)$ = spectral responsivity of the detector in (A/W),

$L_{\lambda,b}(\lambda,T)$ = spectral radiance of the blackbody in $(W/m^2 \cdot \mu m \cdot sr)$,

T = blackbody Temperature (°C),

t_i = optical integration time in (sec),

A_d = area of detector in (m^2),

f/# = f-number of the lens.

By decreasing the optical integration time, the imager can be utilized at higher scene temperatures. However, at lower optical integration times, the NEΔT will be higher for a given temperature. The value of NEΔT as a function of optical integration time t_i and the blackbody temperature T can be expressed as:

$$NE\Delta T(T,t_i) = \frac{\sqrt{N_{IR}^2 + S(T,t_i)}}{\frac{\partial S(T,t_i)}{\partial T}} \qquad (7)$$

where:

N_{IR} = imager readout noise in rms $^{electrons}/_{pixel}$.

In the case of background limited performance (BLIP), the NEΔT as a function of temperature and integration time can be written as:

$$NE\Delta T(T,t_i) = \frac{1}{\sqrt{t_i}} \cdot \sqrt{\frac{4\left(f/\#\right)^2 \cdot 1.6 \times 10^{-19}}{A_d \cdot \Pi}} \cdot \frac{\sqrt{\int_0^\infty R(\lambda)\, L_{\lambda,b}(\lambda,T)\, d\lambda}}{\int_0^\infty R(\lambda)\left(\frac{\partial L_{\lambda,b}(\lambda,T)}{\partial T}\right) d\lambda} \qquad (8)$$

It is interesting to note that the model suggests that the value of NEΔT is inversely proportional to the square root of the optical integration time t_i.

2.5.2 Test Results

Noise measurements were made of a single pixel from the 640 x 480 array at temperatures ranging from 20 to 70°C in the full-frame integration mode and from 100 to 170°C range at the 750 μsec optical integration mode. The signal responsivity was calculated by measuring and plotting the measured pixel voltage at various temperatures. The plot was then analyzed and a second order curve fit was determined. The derivative of this function yields $^{\delta S}/_{\delta T}$ [$^{V}/_{°C}$], the desired result. Noise [rms·mV] was measured at each temperature for that pixel and the quotient of the noise divided by the derivative of the signal at that temperature yields the measured NEΔT. The noise was measured as a peak-to-peak voltage and subsequently divided by five as an approximate rms voltage. Figure 14 shows the modeled performance of the 640 X 480 camera operating with f/#=1.4 optics as a function of temperature for various optical integration times. Overlaid on the graph are the results of measurements taken with the test camera. The error bars shown represent peak-to-peak noise measurements divided by three and six. The solid lines represent the modeled performance while the symbols represent actual data. It is clear from this figure that the camera behaves similarly to the analytic model. Therefore, one may maintain an NEΔT around 0.1°C over the temperature range 25 to 170°C by varying the optical integration time inversely proportionally with optical signal irradiance.

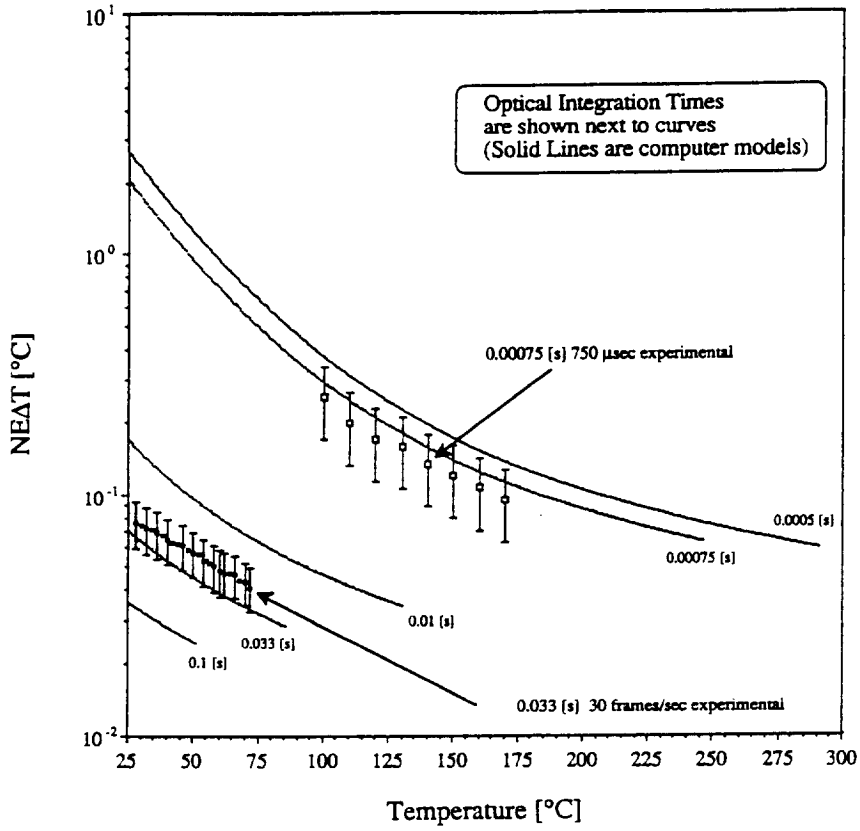

Figure 14. Calculated and measured NEΔT of 640 x 480 IR-MOS imager with f/#=1.4 optics as a function of temperature and optical integration time.

2.6 STABILITY

Stability was studied over both short and long term. The drain current was monitored over long periods of time while staring at a blackbody maintained at a constant temperature. By chopping the optical signal, the short term transient response of the average signal was measured. Also repeated linearity tests of the camera, done on the same day and after thermally cycling the detector, were accomplished to study the reliability of the measurements.

2.6.1 Long Term Drift

Long-term drift was tested by allowing the camera to stare at thirty-five degree radiation for a period of 270 min. and sampling the drain current every 2 min. The measured drain current vs time in minutes is plotted in Fig. 15. It shows that the current varies between 584.1 and 583.2 nA. A smoothed curve is shown superimposed on the data. The solid line in Fig. 15 represents a local averaging of five data points. Shown in the inset of Fig. 15 is a histogram of the acquired data. The rms drift was calculated to be 1.7%. This drift is equivalent to an rms temperature of 6.7 x 10^{-4}°C From the data in Fig. 15, we conclude that the drift of the camera, with respect to photocurrent, is relatively small.

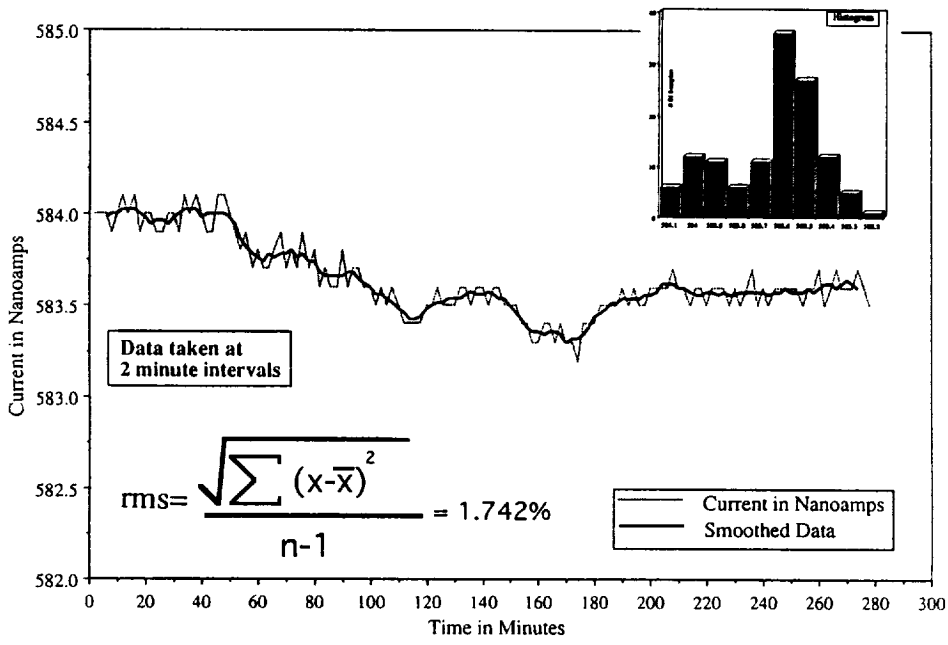

Figure 15. Measured drain current vs time in minutes.

2.6.2 Short Term Transient Response

The short term response was measured by allowing the blackbody to reach a steady state temperature of 35°C and shuttering the light to measure the transient response of the camera. The drain current was monitored by a Houston Instruments (B-5237) 2-pen plotter as a voltage signal acquired from the external port of a Keithley (485) auto-ranging picoammeter. The results are shown in Fig. 16. The camera responds nearly instantaneously with no appreciable settling over 20 sec. We suspect that the small overshoots are due to the mechanical inertia of the plotter pen. Shown in the inset of Fig. 16 is the expansion of the x-axis to show the region from 12 to 15 sec, the response at the point of illumination. These tests show the good temperature response and excellent short term stability of the MOS imager.

2.6.3 Repeatability

Tests were performed to study the repeatability of linearity tests performed repeatedly in one day and tests performed on consecutive days. When the tests were repeated on different days, the temperature of the imaging array was cycled between room and cryogenic operating temperature (77°K). Care was taken not to disturb the test setup, so that the distance from the source to detector and any acute angles measured from the normal of the detector plane would not vary.

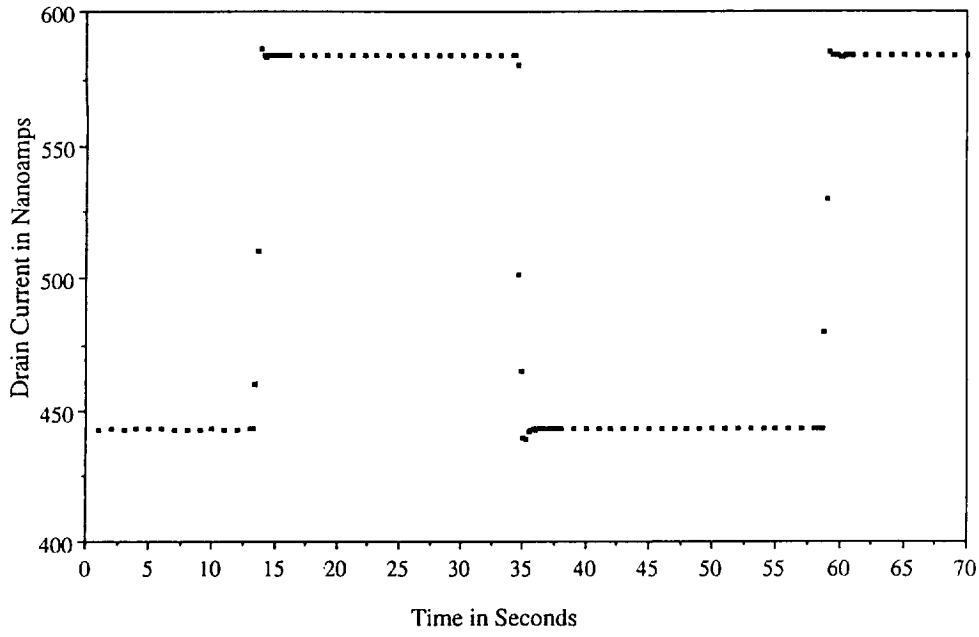

Figure 16. Short term 640 x 480 camera stability/drift.

Three trials were performed on the first day. The average signal was computed as the mean response of the trials. All the current measurements were then converted into detected temperatures and subtracted from the average detected temperature at each optical signal level. This temperature difference was plotted as a function of signal level and is shown in Fig. 17. The results of this test show that the absolute deviation in temperature is approximately ±0.4°C. This instability can be attributed to many factors including blackbody instability, camera electronics and the power supply. Changes in current to changes in temperature illustrate the relative response of the camera. The derivative of the measurements, $\partial I/\partial T$, was subtracted from the derivative of the average response and converted into a percent deviation. This is shown in Fig. 17 and represents the relative response to incremental changes in temperature. The deviations are below ±1% for the measurements shown. The large deviation at low power levels is due to the background signal predominating the scene and introducing nonlinearities in the response.

The results of repeated linearity tests of the 640 x 480 IR-MOS detector are shown in Fig. 18. Tests were taken over a three day period with three tests being performed each day. Figure 18 shows that the effective drift of the camera electronics and instability of the array response due to thermal cycling. Closer inspection of the saturation level in Fig. 18 shows a substantial deviation in the maximum signal level Q_{max}. Since Q_{max} is a function of the reverse bias applied to the PtSi detectors, the deviation shown indicates a drift in the FPA biasing circuits. To eliminate this problem, the FPA biasing circuits are currently being redesigned to incorporate ultra-low drift operational amplifiers and precision voltage reference sources.

(a)

(b)

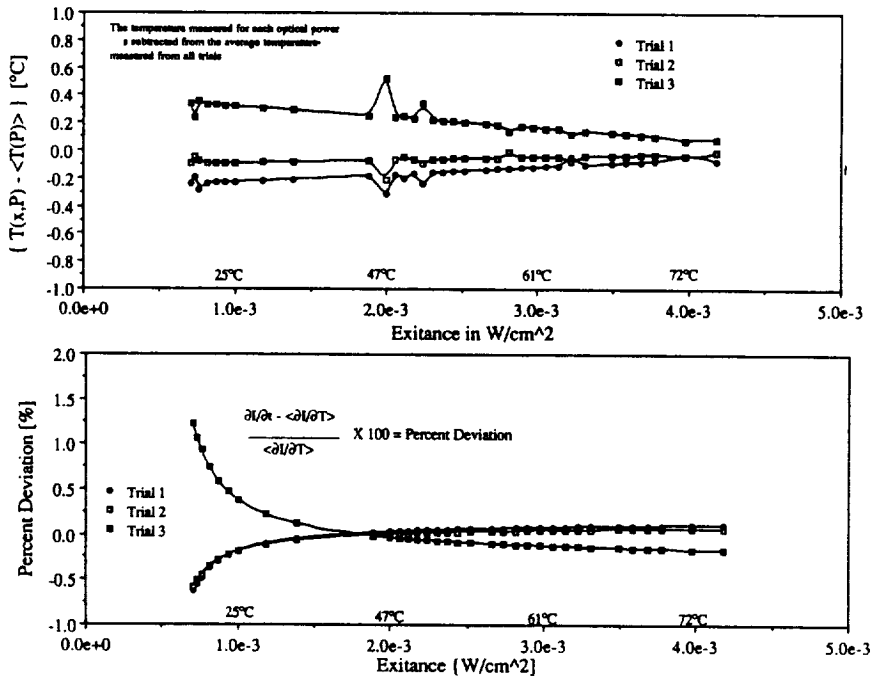

Figure 17. a) Absolute and b) relative temperature deviations vs optical signal.

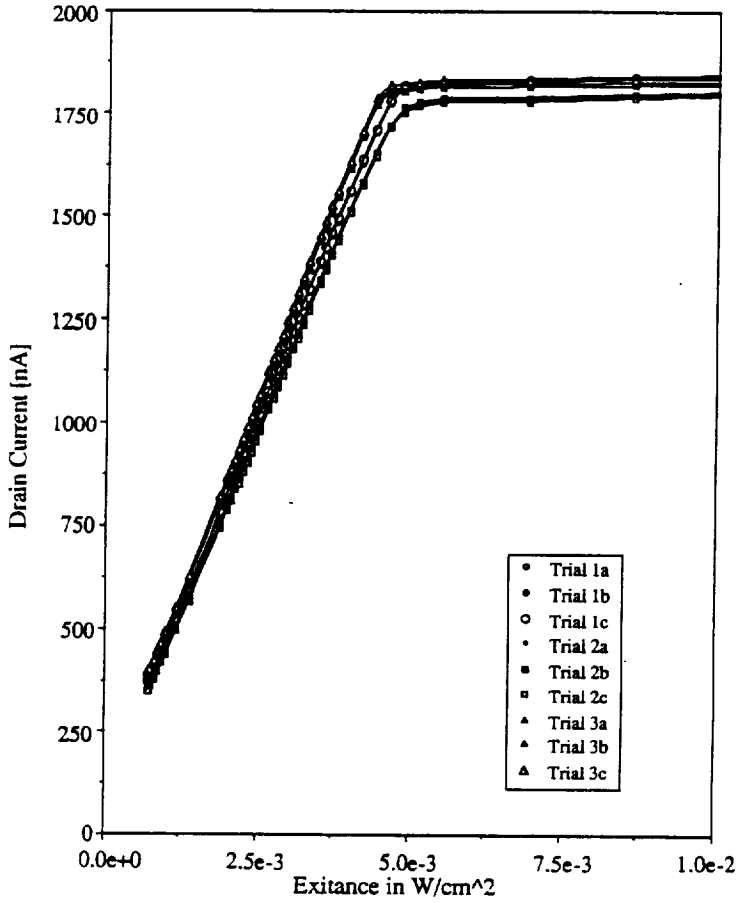

Figure 18. Results of repeated linearity tests of the 640 x 480 IR-MOS detector.

2.7 SUMMARY OF TEST RESULTS

The radiometric evaluation of the 640 x 480 platinum silicide IR-MOS FPA has yielded positive results towards using this camera system for thermography. The linear response of the camera is maintained over the input optical signal level range from 1.7 to 3.7 $^{mW}/_{cm2}$ with less than ±0.3% error from linearity. The pixel to pixel spectral nonuniformity is very low therefore allowing the full spectrum of radiation to be used. The spatial nonuniformities of a two-point corrected imager are a fraction of a percent rms and maintain that low level irrespective of both temperature and input signal level. The NEΔT was successfully modeled and experimental measurements agree reasonably with the model. The NEΔT may therefore be maintained around 0.1°C over the temperature range required by varying the integration time in proportion with the optical signal level. The stability of the camera is good and this study has offered us improvements to the system which will be studied and implemented. Currently, work is underway to improve the biasing circuitry to eliminate drift and improve stability.

On the basis of the experimental results and radiometric analysis, an NEΔT of 0.1°C can be maintained over the full temperature range of 25 to 250°C by operating the camera with variable optical integration time. This operation is shown graphically in Fig. 19 for operation with f/# 1.4 optics. The optical integration times shown vary from 100 to 0.5 millisecond. The curves terminate where saturation of the array occurs. The bold lines represent the integration time required to measure each temperature with an NEΔT around 0.1°C. Therefore to maintain the proper NEΔT, the camera will be operated with integration times from 33 to 0.5 ms. The variation of integration time can be either automatic or preprogrammed. Furthermore, in order to contain the large dynamic range within the same scene (25 to 250°C), the camera will operate with dual (short-long) optical integration times for alternating frames or fields.

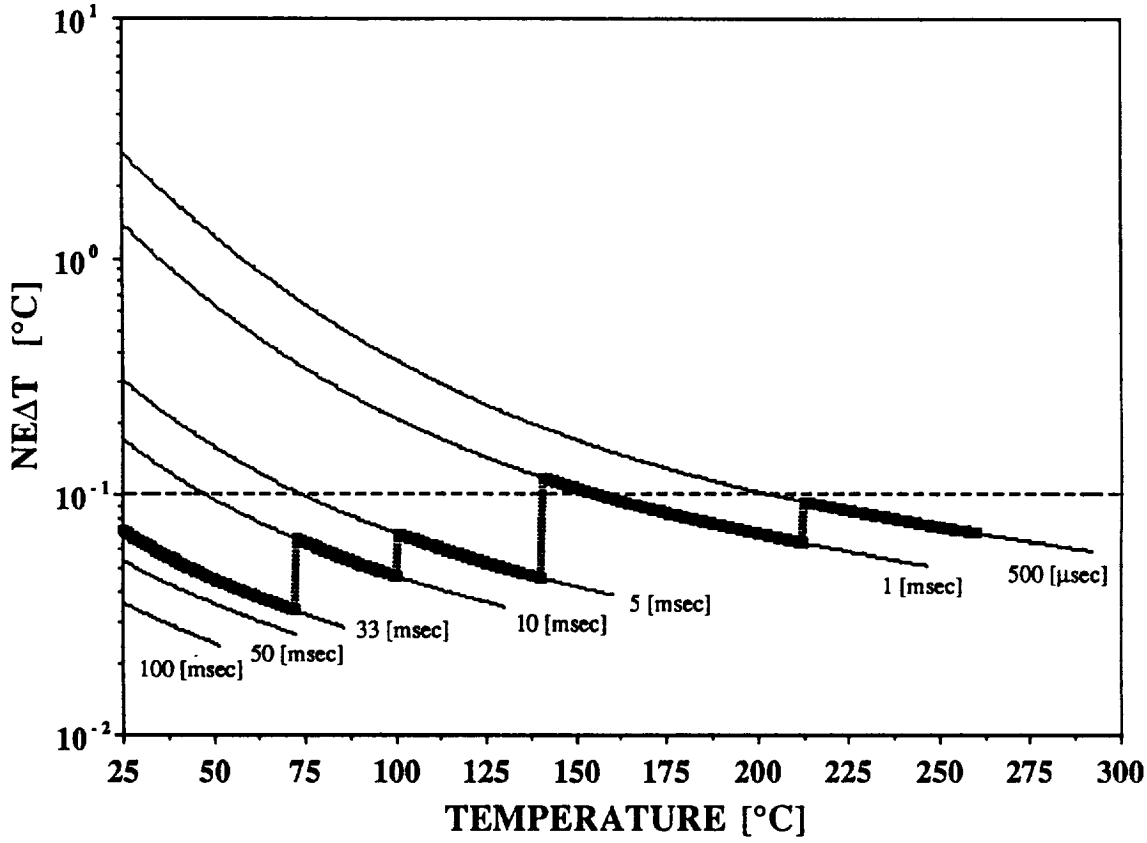

Figure 19. Operation with variable integration time.

3.0 CAMERA DESIGN

This section describes the proposed design and specification of a 640 x 480 PtSi Schottky-barrier IR FPA camera system. The initial goal of this design was to develop a high spatial resolution radiometer with a temperature resolution of 1.0°C or less over the range of 0 to 250C. The proposed camera design developed during this program and described in this report provides: 1) high spatial resolution (full-TV resolution); 2) high thermal dynamic range (0 to 250°C); 3) the ability to image rapid, large thermal transients utilizing electronic exposure control (commandable dynamic range of 2,500,000:1 with exposure control latency of 33 ms); 4) high uniformity (0.5% nonuniformity after correction); and 5) high thermal resolution (0.1°C at 25°C background and 0.5°C at 250°C background).

3.1 SYSTEM OVERVIEW

The proposed camera design described below incorporates wherever possible, existing circuit designs and existing mechanical configurations. A photo of the standard Sarnoff 640 x 480 Stirling cooled camera system is shown in Fig. 20. The camera system shown consists of a camera head and an image processor used for uniformity correction. In response to NASA Langley's requirements, the proposed system for a high resolution radiometer is similar to the system shown except a computer will be used as the system controller and an LN_2 dewar may be substituted for the Stirling refrigerator. A block diagram of the proposed system is shown in Fig. 21. A brief description of each of the system level components is provided below.

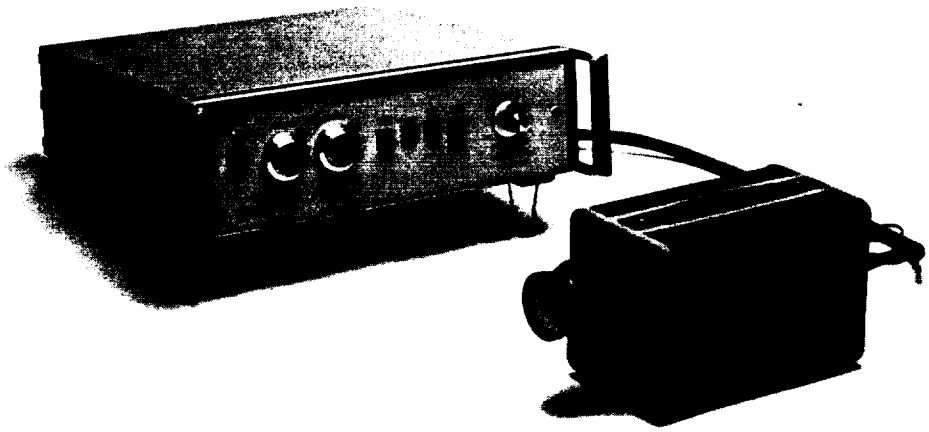

Figure 20. Photograph of the standard Sarnoff 640 x 480 Stirling cooled camera system.

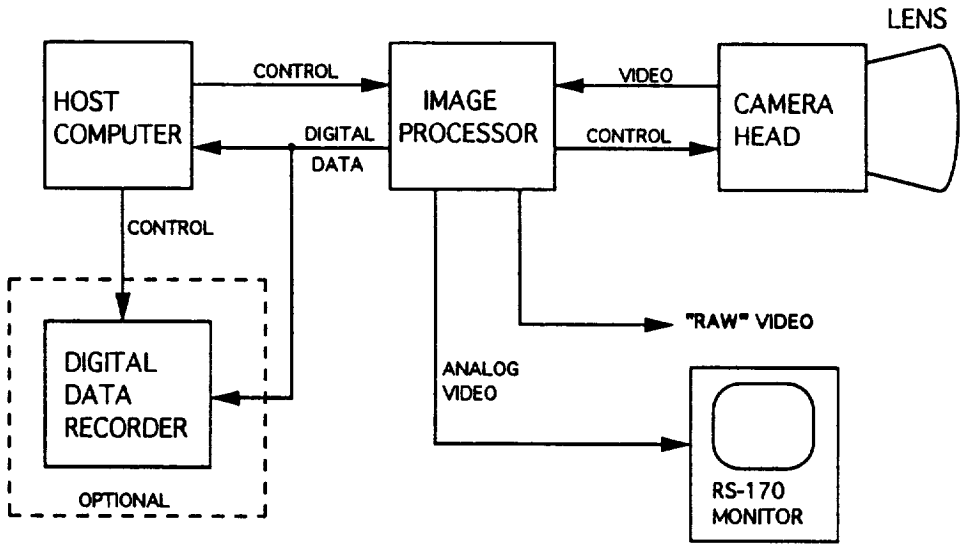

Figure 21. A block diagram of the proposed system.

3.2 SYSTEM CONTROLLER

The system controller will be a personal computer with off-the-shelf cards installed to perform signal processing and data communication. The controller will provide all the necessary commands to run and operate the IR camera system through a standard computer interface. It will also contain a "frame-grabber" board that will accept 12-bit digitized video in real-time for processing and analysis. All system operating parameters will be sent to the computer from the image processor in place of the first few pixels of the first line of video. This allows permanent recording of the system operating parameters of each frame if necessary. Provisions will be made to accommodate the control of the optional digital data recorder.

3.3 CAMERA HEAD

The camera head senses the IR scene and provides analog video and the basic timing signals for the video processor. The camera head includes the FPA mounted in a dewar, a means to cool the FPA to cryogenic temperatures (LN_2 or Stirling refrigerator), and the camera head electronics. A compact camera head will be configured as shown in Fig. 22. The Stirling refrigerator shown can easily be replaced with a LN_2 reservoir if necessary. The diagram illustrates the relationship between the camera head electronics, the dewar assembly, and the mechanical cooler.

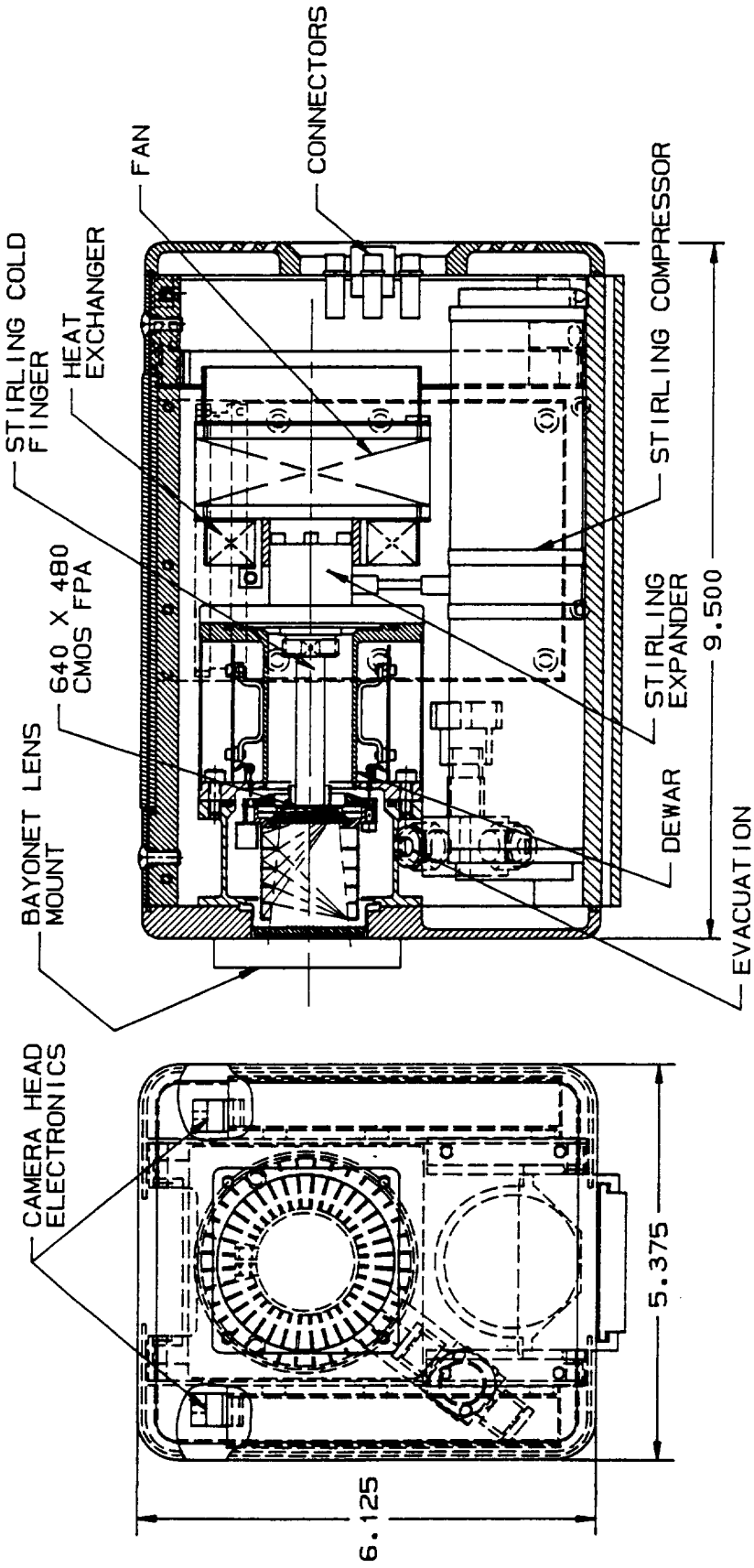

Figure 22. Diagram of the camera head configuration.

The camera head electronics is separated into three sections: the analog processor board, the four dewar interface boards, and the clock generator board. The analog processor board provides amplification and correlated double sampling (CDS) of the FPA video. It also provides 75 ohm buffered drive for the cable between the camera head and image processor. The dewar interface boards provide low level buffering of the analog and digital signals to the FPA, as well as, the initial front end amplification of the FPA output video. The clock generator board generates all the FPA timing pulses which includes the addressing circuitry necessary to implement subframe windowing and electronic exposure control. In addition to full frame (640 x 480) operation at 30 frames/sec, the camera will provide the following subframe rates.

RATE	SUBFRAME SIZE
60 frames/sec	390 x 390
120 frames/sec	275 x 275
240 frames/sec	195 x 195
1000 frames/sec	80 x 80.

Electronic exposure time control will be implemented with the following integration times; 33, 10, 5, 1, 0.5, and 0.25msec. Two separate electronic exposure operational modes will be provided, the single integration mode and the dual integration mode. The single integration mode utilizes a single integration time for processing. This mode would be used when the scene content does not contain a wide dynamic range of temperatures. For scenes that contain wide dynamic temperature ranges, the dual integration mode can be used. The dual integration mode alternates between two integration times at the frame rate. As an example, the camera can be configured to alternate between integration times of 33 msec and 0.5 msec. The 33 msec integration time will allow the most accurate temperature measurements for temperatures $\leq$80°C (saturation occurs at 33 msec for temperatures above this level). The 0.5 msec integration time will provide temperature measurement capability above 80°C to the required maximum temperature of 250°C. Computer image processing software can be developed to merge the data and provide a composite temperature mapping.

The dewar assembly will provide a removable cold shield baffle and a removable cold filter to accommodate various optical system configurations. The cold filter mounting hardware accepts standard 1 in. diameter by 1 mm thick filters. The cold shield baffle is detachable from the cold shield base thus enabling the f/# to be changed if necessary. Changing either the cold shield or the cold filter does not require removing the FPA, and operation can be done within a period of about an hour after proper training.

3.4 IMAGE PROCESSOR

The image processor implements a real time 12-bit image enhancement algorithm and provides the processed data both digitally through a digital output port and as an RS-170 analog output. A functional block diagram of the image processor is shown in Fig. 23. All the necessary controls required to operate the camera system are sent to the image processor from the system controller via a standard computer interface. Video from the camera head is digitized to 12-bits by the A/D converter at the pixel clock rate of 12.2727 MHz. Note that this 12-bit accuracy is carried throughout subsequent processing. The next two blocks in the processing chain, labeled gain correction and offset correction, implement the image enhancement algorithm.

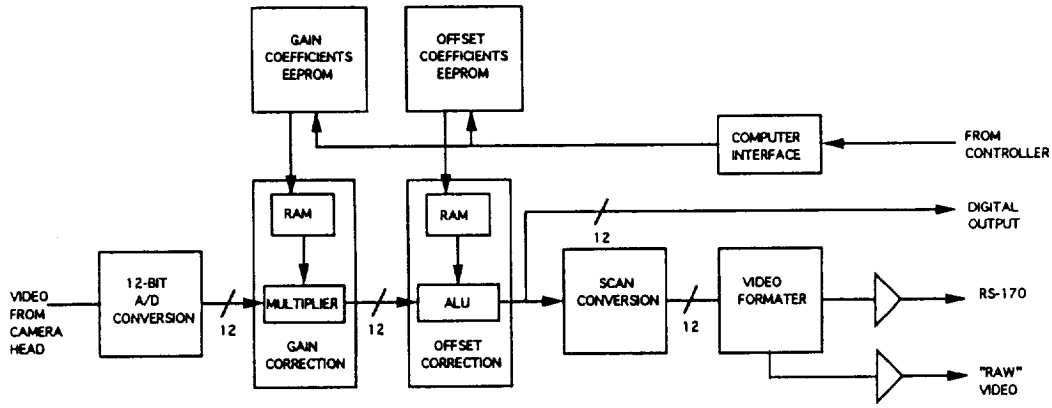

Figure 23. Image processor functional block diagram.

The image enhancement algorithm provides both single-point offset and two-point gain uniformity correction. Without correction the video appears as though the viewer is looking through a dirty window. This effect is caused by variations in dark current and responsivity across the FPA. The single-point offset calibration algorithm averages sixteen frames of a featureless scene and stores the resulting reference frame in memory. This reference frame is subtracted from digitized "live" video to remove pixel-to-pixel dark current variations (offset correction). The two-point gain calibration algorithm will average sixteen frames of two different uniform temperature scenes and calculate the slope of each pixel for the given change in temperature. These results are stored into an additional reference frame and are multiplied by digitized "live" video to remove pixel-to-pixel responsivity variations (gain correction). To accommodate real time calibration, the gain and offset coefficients will be stored in EEPROMs. During operation these coefficients will be loaded into high-speed RAM as required by the pixel data rate.

Not shown explicitly in the block diagram of Fig. 23 is the reinsertion of the offset reference level into the corrected camera signal that preserves the radiometric integrity of the IR camera system (see Section 2.4). This will be accomplished by processing the data in the image

processor or by sending the appropriate coefficients to the system controller where the data will be subsequently processed by the PC.

After uniformity correction the digital data is sent to the scan converter circuitry as well as to a digital output port. The digital output port provides 12-bit data to the system controller for processing. The scan converter circuitry reformats the digital data sequence from progressive scan to the standard RS-170 2:1 interlaced sequence. RS-170 scan conversion will be provided for 30, 60, 120, and 240 frame/subframes rates by displaying every one, 2nd, 4th, and 8th occurring frame/subframe respectively.

The video formatter provides digital offset and gain (for control of the brightness and contrast of the RS-170 analog video), D/A conversion, RS-170 sync insertion, and buffering for a 75 ohm load. In addition, a second analog output will provide "raw" video without sync insertion. This will be the only analog output for the 1000 subframes per second rate.

3.5 OPTICS

The proposed high resolution radiometer will be equiped with a quick-release bayonet mount to accommodate the ability to change lenses quickly. The original specification requested by NASA-Langley had a 40 mm focal length and provided a 20° horizontal by 15° vertical FOV with a depth of field equal to 4 to 6 inches at a distance of 2 ft. The resulting blur spot diameter vs f/number for this lens, is shown in Fig. 24a. Note that the minimum blur spot diameter of 80 μm occurs at f/4 and that it also exceeds the pixel size of 24 μm x 24 μm. The other three graphs shown in Fig. 24 illustrate tradeoffs of depth of focus, working distance, and reduction in focal length to the original specification shown in a. After studying these diagrams graph c provides the optimum compromise in performance at an f/# equal to f/2. At this f/# the blur spot is equal to approximately the pixel size and the optical throughput of the lens has not been significantly compromised.

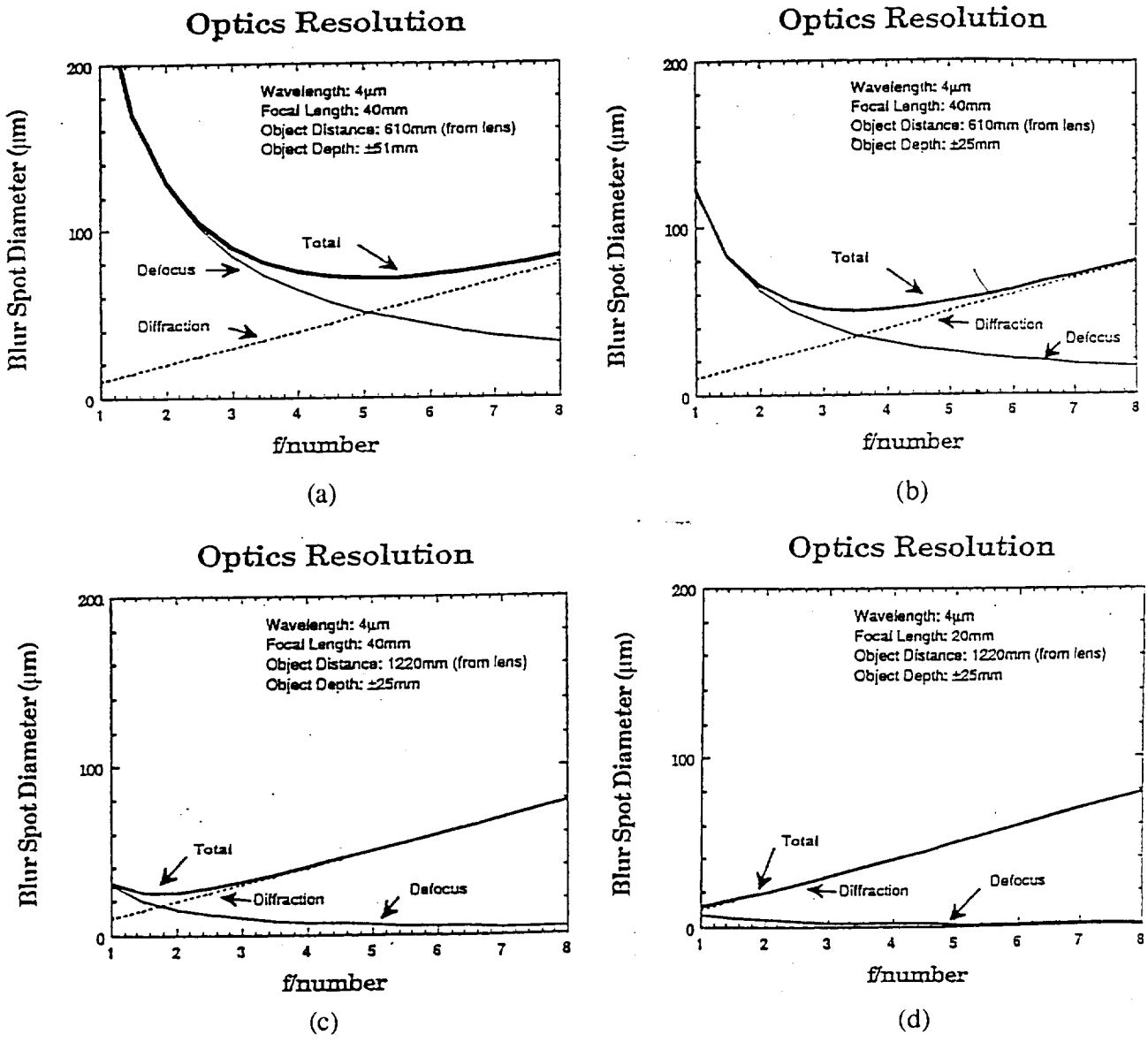

Figure 24. Variation of the blur spot diameter vs the f/# with changes to the origonal design specifications. a) Origonal specifications; b) 50% reduction in depth of focus in (a); c) 2X the working distance from (b); and d) 50% reduction in focal length in (c).

4.0 CAMERA SPECIFICATIONS

The following sections summarize the proposed radiometric camera characteristics and specifications. These characteristics and specifications were developed in close cooperation with NASA-Langley.

4.1 ELECTRICAL OPTICAL SPECIFICATIONS

FPA	640 x 480 PtSi
Pixel Spacing	24 x 24 μm, 38% fill factor
Nonuniformity	0.5% RMS after 2-point correction
Spectral Response	3.4 to 5.5 μm
Pixel Saturation	$1.2e^6$ electrons
Pixel Noise Floor	300 electrons
Instantaneous Dynamic Range	72 dB
Commandable Dynamic Range	124 db
Cold Shield	100% efficient computer designed baffling.
Cold Filter	Standard 1 in. diameter by 1 mm thick. The ability to change cold filters will be provided.
Lens	40mm, f/2 lens providing 20° horizontal by 15° vertical FOV. Bayonet mounted interchangeable lenses in order to have the option to use different focal length or f/# lenses in future.

4.2 RADIOMETRIC SPECIFICATIONS

NETD @ 25°C (measured)	0.08°C
NETD @ 150°C (measured)	0.15°C
Maximum Temperature (33 ms)	75°C
Maximum Temperature (250 μs)	>550°C
Temperature Non-uniformity (@25°C)	<0.1°C (after correction)
Relative Measurement Stability	<0.3%
Absolute Measurement Stability	<±0.4°C

4.3 OPERATIONAL CHARACTERISTICS

Frame rate	30, 60, 120, 240 and 1000 frames/subframes persecond. RS-170 display provided for 30, 60, 120, and 240 frame/subframes per second operation.
Variable Integration	Camera capable of six integration times equal to approximately 33, 10, 5, 1, 0.5, and 0.25 ms for external interscene dynamic range.
Operational modes	(A) Single integration mode: implements a single integration time. (B) Dual integration mode: alternates between two integration times at the frame/subframe rate for external intrascene dynamic range.. In either case the camera output will contain information indicating the integration time for each frame for subsequent processing.
Freeze Frame	Freezes a single frame or subframe upon command.
Inverse Video	Inverts image polarity from "white" hot to "black" hot.
Computer Interface	The camera will interface to a PC which will be used as a controller.
Field Calibration	The camera system will be able to perform bothsingle point (offset) and two point (gain) calibration procedures upon command. The resulting coefficients will be stored in EEPROM.
Digital Output	12-bit digital video with a standard data format that will handshake with off-the-shelf digital image grabbers. System configuration information will be substituted for the values of the first few pixels in the first line.
Analog Outputs	Standard RS-170 format terminated into 75 ohms. Digital offset and gain for display brightness and contrast. "Raw" analog output without sync insertion.
Cooling	LN_2 or Stirling refrigerator
OPTIONS:	
Digital Storage	12-bit digital storage capability of up to 120 consecutive 640 x 480 full frames (55 Mbytes).

5.0 CONCLUSION

A radiometric evaluation of the Sarnoff 640 x 480 PtSi IR-MOS imager concluded that this device can satisfy or exceed all of the requirements specified by NASA Langley for the radiometric imaging system for thermographic applications.

The interscene and intrascene sensitivity and dynamic range requirements for the above imaging radiometer were to achieve an NEΔT of <1% for temperatures in the range of 20 to 200°C. This temperature range corresponds to a 53:1 variation of the IR signal.

To achieve the required interscene dynamic range and to provide operation at relatively constant signal level, the proposed 640 x 480 imaging radiometer will be operated with integration time externally controllable at values of 33, 10, 5, 1, 0.5, and 0.25 ms. To accommodate the 53:1 intrascene variation of the IR signal, the proposed imaging radiometer will be operated in that integration mode for alternate fields or frames.

The radiometric tests of the uncorrected 640 x 480 PtSi IR-MOS imager indicated that its responsivity is linear to $\leq \pm 0.3\%$ for signals up to 83% of the output saturation level. These tests also showed that no observable spectral nonuniformity for individual detectors was found. On the basis of the above results it was concluded that a two-point uniformity correction (for offset and gain) with reinsertion of the offset level will satisfy the required radiometric characteristics for the proposed imaging system.

The above conclusion was verified experimentally for the case where the multiplicative correction coefficients were obtained between reference temperatures T_1=25°C and T_2=30°C and the spatial nonuniformity was measured to be <0.2% rms for the temperature range from 25 to 65°C.

A radiometric analysis of the expected performance of the proposed imaging radiometer indicated that the noise equivalent differential temperature, NEΔT, of 0.1 to 0.2°C can be achieved for scene temperatures ranging from 25 to 250°C by operation of the 640 x 480 imager with the optical integration in the range from 33 to 0.75 ms. The above results were experimentally verified for operation with optical integration time of 33 and 0.75 ms.

While the noise equivalent temperature represents the capability of the proposed imaging radiometer for relative spatial temperature measurements, the absolute temperature measurements will depend on the short-term and the long-term stability of the instrument. The initial measurements of the temperature stability of the test 640 x 480 IR-MOS camera indicated that an absolute temperature resolution <1.0°C should be possible. However, long term stability measurements will be needed in order to make sure that the camera electronics and operating procedures are optimized for reproducible and repeatable radiometric accuracy.

REPORT DOCUMENTATION PAGE

Form Approved
OMB No. 0704-0188

1. AGENCY USE ONLY (Leave blank)	2. REPORT DATE	3. REPORT TYPE AND DATES COVERED
	November 1992	Contractor Report

4. TITLE AND SUBTITLE
Radiometric Infrared Focal Plane Array Imaging System for Thermographic Applications

5. FUNDING NUMBERS
Work Unit No.
307-50-12-06

Contract or Grant No.
NAS1-18226

6. AUTHOR(S)
B. J. Esposito, N. McCaffrey,* R. Brown,
J. R. Tower, W. F. Kosonocky*

7. PERFORMING ORGANIZATION NAME(S) AND ADDRESS(ES)
David Sarnoff Research Center
Princeton, NJ
*New Jersey Institute of Technology
Newark, NJ

8. PERFORMING ORGANIZATION REPORT NUMBER

9. SPONSORING/MONITORING AGENCY NAME(S) AND ADDRESS(ES)
NASA Langley Research Center
Hampton, VA 23665-5225

10. SPONSORING/MONITORING AGENCY REPORT NUMBER
NASA CR-189701

11. SUPPLEMENTARY NOTES
Langley Technical Monitor: Kamran Daryabeigi

12a. DISTRIBUTION/AVAILABILITY STATEMENT
Unclassified - Unlimited
Subject Category 35

12b. DISTRIBUTION CODE

13. ABSTRACT (Maximum 200 words)

This document describes research performed under The Radiometric Infrared Focal Plane Array Imaging System for Thermographic Applications contract. This research investigated the feasibility of using platinum silicide (PtSi) Schottky-barrier infrared focal plane arrays (IR FPAs) for NASA Langley's specific radiometric thermal imaging requirements. The initial goal of this design was to develop a high spatial resolution radiometer with an NETD of 1% of the temperature reading over the range of 0 to 250°C. The proposed camera design developed during this study and described in this report provides: 1) high spatial resolution (full-TV resolution); 2) high thermal dynamic range (0 to 250°C); 3) the ability to image rapid, large thermal transients utilizing electronic exposure control (commandable dynamic range of 2,500,000:1 with exposure control latency of 33 ms); 4) high uniformity (0.5% nonuniformity after correction); and 5) high thermal resolution (0.1°C at 25°C background and 0.5°C at 250°C background).

14. SUBJECT TERMS
Radiometry
PtSi Focal Plane Array
Infrared Camera

15. NUMBER OF PAGES
38

16. PRICE CODE
A03

17. SECURITY CLASSIFICATION OF REPORT	18. SECURITY CLASSIFICATION OF THIS PAGE	19. SECURITY CLASSIFICATION OF ABSTRACT	20. LIMITATION OF ABSTRACT
Unclassified	Unclassified	Unclassified	Unlimited